 ©2021 Kvantovaya Elektronika and IOP Publishing Limited

https://doi.org/10.1070/QEL17537

Recognition of individual scatterers against the noise background in the optical coherence tomography image

P.A. Shilyagin, A.A. Novozhilov, A.L. Dilenyan, T.V. Vasilenkova, A.A. Moiseev, I.V. Kasatkina, V.M. Gelikonov, G.V. Gelikonov

Abstract. **The problem of recognising single sparsely located scatterers against the noise background in the image obtained by the method of optical coherence tomography (OCT) is considered. An identification method based on the use of specific scanning features upon OCT image registration and on the statistical analysis of image fragments is proposed. The efficiency of the method is demonstrated experimentally in the diagnosis of otitis media with effusion. The approach can be used in the development of automated algorithms for determining the presence of highly transparent effusion in the middle ear cavity of a human with acute otitis media with effusion, including postoperative one.**

Keywords: *optical coherence tomography, otitis media with effusion, noninvasive diagnostics, medical biophotonics, common optical path scheme.*

1. Introduction

Optical coherence tomography (OCT) has become widespread as a method of biomedical imaging due to the noninvasiveness of the procedure and high spatial resolution compared to ultrasonic imaging. The combination of these properties, together with the possibility of unhindered propagation of probing radiation in the optically transparent medium of the vitreous body, made the OCT technology a 'gold standard' in ophthalmology, primarily in the study and diagnosis of retinal diseases. At the same time, in the minds of the clinical community, ophthalmoscopy has established itself as a preferred field for OCT application. However, starting from the earliest stages of its development, OCT was also used to study other organs and tissues, giving rise to independent directions of endoscopic, vascular and superficial OCT.

One of the promising directions in the development of technology for clinical application is the use of OCT in the examination of the hearing organs, primarily the tympanic membrane (TM) and the tympanic cavity (TC). Publications of 2010–2016 showed the possibility of optical detection of biofilms on the inner side of the TM [1, 2] and the accumulation of liquid behind the TM [3–5], and also announced the possibility of assessing the viscosity of this liquid [6] from the OCT data. The possibility of direct OCT imaging of the TC contents opens up new perspectives for the timely diagnosis of such a difficult-to-detect disease as otitis media with effusion (OME).

Otitis media with effusion is a non-suppurative disease of the middle ear, which is characterised by the accumulation of fluid (exudate, effusion) in the TC due to a violation of its natural outflow through the Eustachian tube. The accumulation of fluid in the TC leads to a limitation of the TM mobility, which, in turn, manifests itself in a gradual hearing loss as the TC fills. The absence of pain and the smoothness of the development of OME, as a rule, lead to a general neglect of the disease at the time of detection. This circumstance not only has independent negative consequences (adhesive otitis media, retraction pockets, tympanosclerosis, cholesteatoma and sensorineural hearing loss [7–11]), but also significantly increases the likelihood of the need for surgical intervention (tympanostomy). Moreover, pronounced hearing impairment in newborns and children of the first years of life deserves special attention, because in the absence of sounds and speech, the verbal type of thinking is not formed. This leads to serious impairments in the formation of speech and thinking and, as a result, to developmental delays.

The currently existing methods for determining the presence of fluid in the TC have low sensitivity and specificity. Thus, for standard otoscopy (visual observation), these figures are 74%–87% and 60%–74%, respectively [12–14]. The sensitivity of tympanometry, a method based on determining TM mobility, is slightly higher. According to the data of Refs [15, 16], the sensitivity of tympanometry is 85.5% and the specificity is 72%, which is due to the possibility of limiting TM mobility not only due to the accumulation of fluid in the TC. At the same time, in a number of cases, the use of additional diagnostic methods turns out to be difficult due to the inaccessibility of the external auditory canal (EAC) for sealing or painfulness of the procedure for the patient, in particular, with the development of postoperative OME. The possibility of hearing loss up to its complete absence as a result of damage to the auditory nerve or the development of OME due to infection with SARS-CoV-2 (Covid-19) deserves special mention [17–21]. In this case, there is a special need to minimise both the number of diagnostic procedures and the medical personnel involved in them.

The sensitivity and specificity of OCT in relation to the detection of fluid in the TC already in the first studies exceeded

P.A. Shilyagin, T.V. Vasilenkova, A.A. Moiseev, I.V. Kasatkina, V.M. Gelikonov, G.V. Gelikonov Institute of Applied Physics, Russian Academy of Sciences, ul. Ulyanova 46, 603950 Nizhny Novgorod, Russia; e-mail: grgel@yahoo.com;
A.A. Novozhilov, A.L. Dilenyan Institute of Applied Physics, Russian Academy of Sciences, ul. Ulyanova 46, 603950 Nizhny Novgorod, Russia; Volga District Medical Centre, Federal Medical-Biological Agency, Nizhnevolzhskaya nab. 2, 603001 Nizhny Novgorod, Russia

Received 16 February 2021
Kvantovaya Elektronika **51** (5) 371–376 (2021)
Translated by V.L. Derbov

90%. The data published in early 2020 [22] demonstrate the sensitivity and specificity of the method ~91% and ~90%, respectively. In this case, the repeatability of the expert assessment for each case was~87%. The study was characterised by the subjectivity of the assessment of each clinical case (the assessment was carried out only visually) and the limited information provided. One B-scan (two-dimensional image of the examined tissue cross-section) was presented, containing the TM, TC and EAC areas.

This paper is devoted to the development of methods for increasing the sensitivity of OCT with respect to fluid detection in the TC.

2. Materials and methods

2.1. OCT system

OCT data were recorded using a system described in detail in Ref. [23] (Fig. 1), equipped with replaceable sterile attachments (standard otoscopic mirrors). The centre wavelength of the probe radiation is 1.3 μm, the optical spectrum recording bandwidth is 80 nm, and the acquisition rate of A-scans (the primary lines of the OCT image corresponding to the recorded scattering profile of the object at one position of the probe beam) is 2×10^4 s^{-1}. The spectrally conditioned resolution is 11 μm, and the maximum imaging depth in one frame is 3.2 mm. The data is presented in a quasi-volumetric image format composed of 1024 separate B-scans taken sequentially at 25 ms intervals.

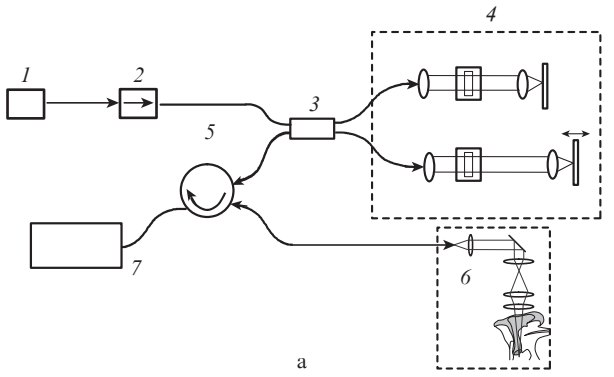

a

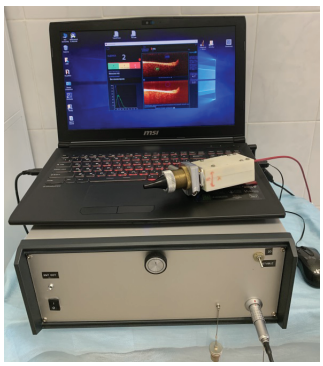

b

c

Figure 1. (a) Schematic of the experimental OCT system, (b) its appearance, and (c) a photograph of the OCT examination procedure: (*1*) broadband light source; (*2*) optical isolator; (*3*) 50/50 splitter; (*4*) additional fibre Michelson interferometer; (*5*) optical circulator; (*6*) scanner (basic Fizeau interferometer); (*7*) spectrometer.

The system is based on the Fizeau interferometer (*6*) (Fig. 1a) [24], formed by two objects – the scatterers of the medium under study and the end face of the optical fibre in the probe, which makes it possible to implement a common optical path for the reference and probe waves. The use of such an optical design makes it possible to prevent the occurrence of undesirable polarisation distortions caused by bending deformations of the optical fibre and characteristic of Michelson or Mach–Zehnder interferometers. The optical delay in the basic Fizeau interferometer with a length of more than 20 cm is compensated for by switching on an additional Michelson fibre interferometer (*4*) with the same shoulder difference. The use of Faraday mirrors makes it possible to eliminate the polarisation anisotropy of the optical fibre in the arms of the Michelson interferometer. In addition, the compensating interferometer implements subwavelength modulation of the optical path difference, which is necessary for effective suppression of the autocorrelation component of the interferometric signal [25–27]. The high level of linearity of the spectrometer dispersion characteristics (maximum deviation less than 0.01%) required for high-performance digital processing of the OCT signal is ensured by using a composite dispersion element [28].

For streaming processing of registered images, specialised software AnalysEar (Institute of Applied Physics, RAS, Russia) was developed, which allows both visualising the obtained data and performing its statistical processing (calculating the mean, variance, arbitrary percentiles of the brightness distribution in the selected area) with the possibility to transfer information to the third-party software.

2.2. Clinical material and obtaining OCT data

Clinical material for the study was collected in 2018–2019 in the ENT department of the Volga District Medical Centre of the Federal Medical and Biological Agency of Russia with the approval of the local Committee on Research Ethics of the Privolzhsky Research Medical University of the Ministry of Health of Russia (Protocol No. 7 of 03.07.2017). OCT data were recorded in patients with confirmed OME, to whom tympanostomy was recommended on the base of the results of the application of the basic diagnostic standards. The presence of exudate in the TC and its qualitative characteristics were verified by the results of tympanostomy

3. Analysis of OCT data

The presence of exudate in the TC is identified on OCT images by the presence of a signal in the TC region, which cannot be attributed to artefacts or elements of the structure (tissues) of the middle ear.

The characteristics of the exudate signal in the OCT image in the TC are determined by its qualitative and quantitative compositions. In an acute course and a short duration of the disease, the exudate, as a rule, is a predominantly transparent liquid with a low viscosity, which may contain individual scattering elements (Figs 2a and 2b). In the micrograph shown in Fig. 2a, individual cells are identified in the field of view, with a high probability living ones. In other cases, the presence of other relatively large structures (significantly exceeding the wavelength of the probe radiation) – cellular debris and tissue fragments – is noted. Due to the high transparency of the exudate and the low concentration of scatterers in the TC region of the OCT image, the average brightness differs

little from the noise one (the reference image is taken to be the region corresponding to the EAC). However, with varying degrees of confidence, individual bright inclusions are detected as a scattering signal from micro-objects, suspended in liquid.

For a protracted and chronic course of OME, the presence of exudate with a high viscosity in the TC is more characteristic due to the presence of a large number of massive molecules in it [29, 30]. In this case, an increase in the concentration of large scattering centres (cells, etc., see Fig. 2c) is also often noted. The presence of supermassive organised molecules and an increased concentration of individual scatterers lead to a significant increase in the average brightness in the TC (Fig. 2d) [31]. This allows not only diagnosing the presence of exudate in the TC, but also assessing its viscosity, based on data on the backscattering intensity.

The main reason for the decrease in the OCT sensitivity in relation to the determination of the presence of liquid in the TC is the difficulty of detecting individual scatterers upon their low volume concentration in the transparent exudate. In this case, scatterers may not be present on every B-scan, and the low backscattering coefficient may not allow recognising the scatterer against the noise background. The latter is primarily due to the small gradient of the refractive index at the boundary between the cellular fragment and the liquid medium, as well as the small sizes of scattering objects [in Fig. 2a for comparison, a scale element is shown corresponding to the diameter of the probe beam (25 μm)]. To increase the probability of detecting rare single inclusions, in this work, we use two methods: a multiple increase in the investigated volume of the TC by analysing a series of sequentially obtained B-scans and highlighting the features of the brightness distribution characteristic of the presence of scatterers in the OCT image.

A multiple increase in the investigated volume of the TC is realised by constructing a maximum intensity projection (MIP) on a fixed plane for a certain number of sequentially obtained B-scans. Without changing the two-dimensional format of the result presentation, this approach allows simultaneous visualisation of all individual scatterers contained in the investigated volume. The applicability of the method is limited to 10–20 sequential B-scans, which is due to the TM curvature, which leads to a visual thickening of this membrane in MIP images. An example of using this approach is presented in Fig. 3, which shows a clinical case of a liquid transparent exudate that filled the entire TC. The volume concentration of scattering particles is $\sim 10^3\ \mu L^{-1}$, as a result of which one or two scatterers are recorded on average in one B-scan (the total volume without taking into account the refractive index of the medium is $2 \times 10^{-3}\ \mu L^{-1}$) (Fig. 3a). An increase in the visualised volume by a factor of 20 due to the formation of MIP images leads to a corresponding increase in the number of observed scatterers. In this case, each fragment of the scatterer image is displayed with the maximum registered brightness. Such scatterers become more contrasting against a substantially evened noise background.

An important factor for increasing the diagnostic sensitivity of biomedical imaging methods is the development of automated approaches for identifying significant features in

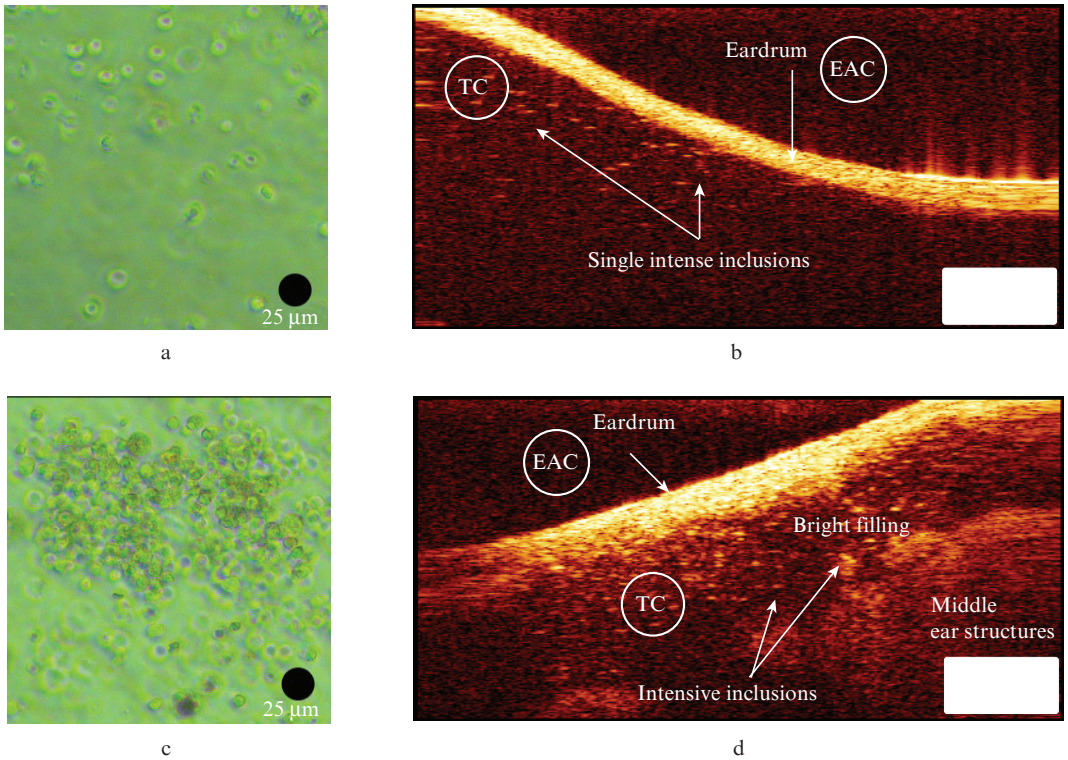

Figure 2. (Colour online) Middle ear exudate: (a) a microscopic image of a liquid exudate with single scatterers and (b) its OCT image in the TC, as well as (c) a microscopic image of a viscous exudate and (d) its OCT image in the TC. The bar size in the OCT images is 500 × 500 μm.

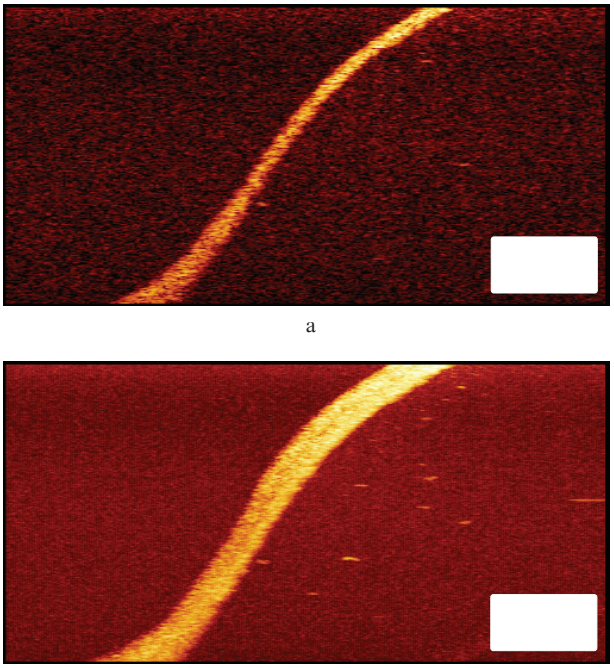

Figure 3. (Colour online) OCT images of a TC filled with liquid exudate: (a) a single B-scan and (b) an MIP image obtained from 20 consecutive B-scans. The bar size in the OCT images is 500 × 500 μm.

the array of recorded data. Within the framework of the problem under consideration, a method was developed that would allow analysing the nature of the distribution of image brightness in the vicinity of local maxima associated with the specific features of transverse scanning in the experimental system. Due to the need to correct the influence of autocorrelation artefacts (known as 'mirror artefacts'), which are inevitable in the imaging with a wide dynamic range [32–34], as well as physiologically determined mutual displacements of the object and the OCT probe [35], transverse scanning was performed with significant overlap of the scanning beam profiles. As a result, each scatterer contributes to the formation of several sequentially recorded A-scans. This, in turn, leads to the fact that, in contrast to the uncorrelated background noise caused by the shot noise of the receiver and the excess noise on the photodetector [36], the image of a conditionally point (smaller than the probe beam diameter) scatterer demonstrates a high degree of brightness correlation in adjacent lines of the OCT image. In this case, the brightness for neighbouring scans has close values due to using a logarithmic scale when converting the scattering signal into the image brightness. An example of an OCT image of a TC filled with a transparent exudate with single isolated scatterers and a magnified image of such a scatterer are shown in Fig. 4a.

Statistical processing makes it possible to determine the width of the noise distribution in the image region corresponding to the EAC, which, together with the determination of the position of the distribution centre, makes it possible to normalise the recorded scattering signal. Figure 4,b shows

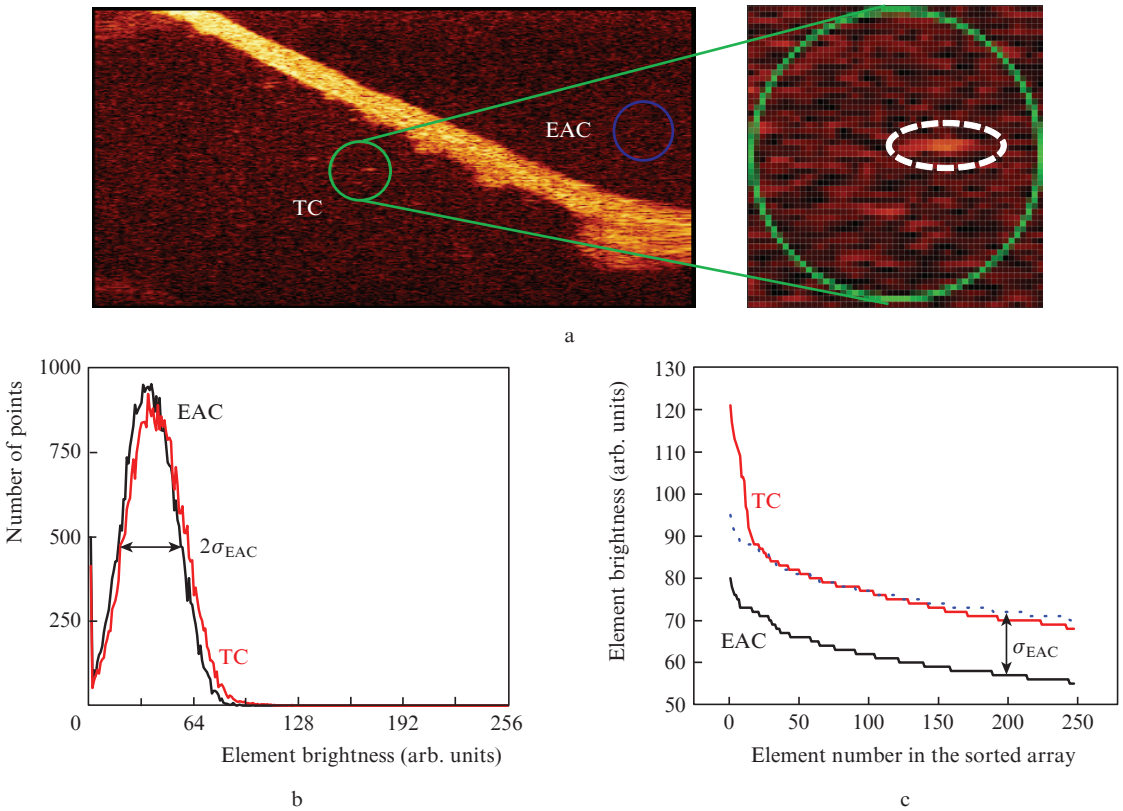

Figure 4. (Colour online) (a) OCT image of a TC filled with liquid exudate, as well as (b) a distribution histogram and (c) sorted values of brightness in the selected areas of TC and EAC. The magnified fragment of the image contains an identifiable scatterer (inside the white dashed line).

brightness distribution histograms for the regions corresponding to the EAC and TC, plotted from 20 consecutive B-scans. It can be seen that the TC histogram has a noticeable shift relative to the EAC histogram, which may indicate the presence of low-intensity scatterers in the analysed region. However, the magnitude of this shift is significantly less than the width of the noise distribution; therefore, the indicated shift is not sufficient to determine the presence of a liquid medium behind the TM reliably. Moreover, the features of signal registration in OCT do not exclude the possibility of registering multiply scattered photons, which, due to the increase in the length of the trajectories, also gives rise to a phantom increase in the image brightness behind strongly scattering objects.

The essence of the proposed method is that to detect the presence of individual scatterers behind a scattering object, it is proposed to use the analysis of the brightness of individual elements, for which the array of data included in the selected area is sorted in order of decreasing element brightness. The result of such sorting for arrays corresponding to the selected areas in the EAC and TC is shown in Fig. 4c. Additionally, a reference dashed curve is also presented, calculated as the sum of the brightness of an element in the EAC and the half-width of the brightness distribution of the noise signal σ_{EAC}. In the magnified fragment of the image in Fig. 4a, it can be seen that the total number of image points retaining information on the presence of a scatterer is $\sim$20. This result is typical for most of the analysed OCT images; deviations are found only upward, which is due to the location of the scatterers outside the region of maximum focusing of the probe radiation or their larger sizes. The effect of Brownian motion, which potentially destroys the correlation for images of individual scatterers in the case of sequential registration of image lines, at the realised A-scan registration rate of 2×10^4 s^{-1} can be neglected [6, 37]. We conclude that exceeding the level defined as the sum of the EAC point brightness and the noise distribution half-width by more than five to ten successive elements of the sorted brightness distribution in the TC region can be considered sufficient to conclude that there are scatterers in the analysed region, and hence exudate in the TC.

4. Approbation of the method on real data

For experimental testing of the proposed method for detecting exudate in the TC, its sensitivity and specificity were assessed by independent experts. The experts were provided with OCT data with the possibility to construct MIP images and perform digital analysis of the local brightness distribution. Analysis of the proposed method sensitivity and specificity for evaluating OCT data with the purpose to detect exudate showed high values of these indicators, 98% and 90%, respectively. In a subgroup of experts with significant experience of working with OCT, the described technique demonstrated a diagnostic accuracy close to 100%. The results obtained are much better than in Ref. [22], which, most likely, is due precisely to the increase in the sensitivity of the technique for liquid exudates with high transparency.

5. Conclusions

The developed method for evaluating OCT data, which consists in providing the operator with the possibility of visualising, in addition to the main image, also the MIP image synthesised from several sequentially obtained B-scans, showed highly efficient detection of a liquid in the TC. The sensitivity and specificity of the approach, demonstrated during its experimental testing, significantly exceed both similar indicators for standard diagnostic methods and previously published values for OCT.

An effective study volume is critically important in the analysis of OCT data obtained from the TC, which makes it possible to detect exudates with a high degree of transparency, including those characteristic of postoperative cases of OME.

Acknowledgements. The work was supported by the World-Class Research Centre "Photonics Centre" under the financial support of the Ministry of Science and High Education of the Russian Federation (Agreement No. 075-15-2020-906).

References

1. Nguyen C.T., Tu H., Chaney E.J., Stewart C.N., Boppart S.A. *Biomed. Opt. Express*, **1**, 1104 (2010).
2. Nguyen C.T., Robinson S.R., Jung W., Novak M.A., Boppart S.A., Allen J.B. *Hearing Res.*, **301**, 193 (2013).
3. Meller A., Shakhova M., Rilkin Y., Novozhilov A., Kirillin M., Shakhov A. *Photonics Lasers Med.*, **3**, 323 (2014).
4. Cho N.H., Lee S.H., Jung W., Jang J.H., Kim J. *J. Korean Med. Sci.*, **30**, 328 (2015).
5. Novozhilov A.A., Shakhov A.V. *Folia Otorhinolaryngol.*, **22**, 46 (2016).
6. Monroy G.L., Pande P., Shelton R.L., Nolan R.M., Spillman D.R. Jr., Porter R.G., Novak M.A., Boppart S.A. *J. Biophotonics*, **10**, 394 (2017).
7. Tos M., Stangerup S.E., Larsen P. *Acta Otolaryngol.*, **112** (3), 512 (1992).
8. Tos M., Stangerup S.E., Larsen P. *Arch. Otolaryngol. Head Neck Surg.*, **113**, 380 (1987).
9. Wilhelm T., Stelzer T., Hagen R. *Ear Nose Throat J.*, **95**, E18 (2016).
10. Mileshina N.A., Volodkina V.V. *Ross. Otorinolaringol.*, **5**, 97 (2008).
11. Savenko I.V., Boboshko M.Yu., Lopotko A.I., Tsvyleva I.D. *Ekssudativnyi srednii otit* (Otitis media with effusion) (St. Petersburg: Dialog, 2010) p. 80.
12. Kaleida P.H., Stool S.E. *Am. J. Dis. Child.*, **146**, 433 (1992).
13. Lee D.-H., Yeo S.-W. *J. Korean Med. Sci.*, **19**, 739 (2004).
14. Harris P.K., Hutchinson K.M., Moravec J. *Am. J. Audiol.*, **14**, 3 (2005).
15. Taiji H., Kanzaki J. *Nippon Jibiinkoka Gakkai Kaiho*, **119**, 727 (2016).
16. Sharma K., Pannu M.S., Arora A., Sharma V. *Indian J. Otolaryngol. Head Neck Surg.*, **68**, 163 (2016).
17. Koumpa F.S., Forde C.T., Manjaly J.G. *BMJ Case Reports*, **13**, e238419 (2020).
18. Karimi-Galougahi M., Naeini A.S., Raad N., Mikaniki N., Ghorbani J. *Acta Otorhinolaryngol. Ital.*, **40** (6), 463 (2020).
19. Kilic O., Kalcioglu M.T., Cag Y., Tuysuz O., Pektas E., Caskurlu H., Cetın F. *Int. J. Infect. Dis.*, **97**, 208 (2020).
20. Munro K.J., Uus K., Almufarrij I., Chaudhuri N., Yioe V. *Int. J. Audiol.*, **59**, 889 (2020).
21. Fraczek M., Resler K., Szetela B. *Hearing J.*, **73**, 8 (2020).
22. Preciado D., Nolan R.M., Joshi R., Krakovsky G.M., Zhang A., Pudik N.A., Kumar N.K., Shelton R.L., Boppart S.A., Bauman N.M. *Otolaryngol. Head Neck Surg.*, **162**, 367 (2020).
23. Shilyagin P.A., Novozhilov A.A., Abubakirov T.E., Dilenyan A.L., Shakhov A.V., Moiseyev A.A., Terpelov D.A., Ksenofontov S.Yu., Matkivskiy V.A., Gelikonov V.M., Gelikonov G.V. *Quantum Electron.*, **51** (1), 38 (2021) [*Kvantovaya Elektron.*, **51** (1), 38 (2021)].
24. Gelikonov V.M., Gelikonov G.V., Shilyagin P.A. *Bull. Russ. Acad. Sci., Ser. Phys.*, **72** (1), 93–97 (2008) [*Izv. Ross. Akad. Nauk, Ser. Fiz.*, **72**, 104 (2008)].

25. Gelikonov V.M., Gelikonov G.V., Ksenofontov S.Yu., Terpelov D.A., Shilyagin P.A. *Instrum. Exp. Tech*., **53**, 443 (2010) [*Prib. Tekh. Eksp*., **53**, 443 (2010)].
26. Gelikonov V.M., Gelikonov G.V., Terpelov D.A., Shabanov D.V., Shilyagin P.A. *Quantum Electron*., **42**, 390 (2012) [*Kvantovaya Elektron*., **42**, 390 (2012)].
27. Ksenofontov S.Yu., Shilyagin P.A., Terpelov D.A., Novozhilov A.A., Gelikonov V.M., Gelikonov G.V. *Instrum. Exp. Tech*., **63**, 126 (2010) [*Prib. Tekh. Eksp*., **63**, 136 (2020)].
28. Shilyagin P.A., Ksenofontov S.Yu., Moiseyev A.A., Terpelov D.A., Matkivskiy V.A., Kasatkina I.V., Mamaev Ya.A., Gelikonov G.V., Gelikonov V.M. *Radiophys. Quantum Electron*., **60**, 769 (2018) [*Izv. Vyssh. Uchevn. Zaved., Ser. Radiofiz*., **60**, 859 (2017)].
29. Preciado D., Goyal S., Rahimi M., Watson A.M., Brown K.J., Hathout Y., Rose M.C. *Pediatr. Res.*, **68**, 231 (2010).
30. Val S., Poley M., Anna K., Nino G., Brown K., Pérez-Losada M., Gordish-Dressman H., Preciado D. *Pediatr. Res*., **84**, 296 (2018).
31. Novozhilov A.A., Shilyagin P.A., Abubakirov T.E., Dilenyan A.L., Klimycheva M.B., Gelikonov G.V., Ksenofontov S.Yu., Gelikonov V.M., Shakhov A.V. *Vestnik Otorinolaringol.*, **85**, 16 (2020).
32. Davis B.J., Ralston T.S., Marks D.L., Boppart S.A., Carney P.S. *Opt. Lett*., **32**, 1441 (2007).
33. Gelikonov V.M., Gelikonov G.V., Kasatkina I.V., Terpelov D.A., Shilyagin P.A. *Opt. Spectrosc*., **106**, 895 (2009) [*Opt. Spektrosk*., **106**, 983 (2009)].
34. Steiner P., Meier C., Koch V.M. *Appl. Opt*., **49**, 6917 (2010).
35. Gelikonov G.V., Ksenofontov S.Yu., Shilyagin P.A., Gelikonov V.M. *Radiophys. Quantum Electron*., **62**, 228 (2019) [*Izv. Vyssh. Uchebn. Zaved., Ser. Radiofiz*., **62**, 252 (2019)].
36. Gelikonov V.M., Romashov V.N., Gelikonov G.V. *Quantum Electron*., **51**, 377 (2021) [*Kvantovaya Elektron*., **51**, 377 (2021)].
37. Shilyagin P.A., Novozhilov A.A., Abubakirov T.E., Gelikonova V.G., Terpelov D.A., Matkivsky V.A., Gelikonov G.V., Shakhov A.V., Gelikonov V.M. *Laser Phys. Lett.*, **15**, 096201 (2018).